International Journal of Control, Automation, and Systems (2015) 13(3):503-512 ISSN:1598-6446 eISSN:2005-4092
DOI 10.1007/s12555-014-0251-9 http://www.springer.com/12555

High-speed Train Navigation System based on Multi-sensor Data Fusion and Map Matching Algorithm

Kwanghoon Kim, Sanghwan Seol, and Seung-Hyun Kong*

Abstract: Navigation system for high-speed trains is necessary for increased operational safety and efficiency, new services for customers, and low maintenance cost. This paper proposes a high accuracy navigation system for high-speed trains based on a sensor fusion algorithm, with non-holonomic constraints, for multiple sensors, such as accelerometers, gyroscopes, tachometers, Doppler radar, differential GPS, and RFID, and a map matching algorithm. In the proposed system, we consider the federated Kalman filter for sensor fusion, where local filters utilize filter models developed for various sensor types. Especially, the local Kalman filter for RFID positioning, that is detected at irregular time intervals due to the varying train speed and RFID tag spacing, is developed to maintain high performance during GPS outage. In addition, an orthogonal projection map matching algorithm is developed to improve the performance of the proposed system. The performance of the proposed system is demonstrated with numerous simulations for a high-speed train in Korea. The simulation results are analyzed with respect to the existence of tunnel, RFID deployment spacing, RFID location uncertainty, and DGPS error.

Keywords: Federated Kalman filter, map matching, multisensor fusion, train navigation system.

1. INTRODUCTION

Conventional train navigation systems have been used for train control to prevent train collision and for efficient train operation and scheduling [1,2]. In the rail industry, track circuits and tachometers are used in conventional train navigation systems. The track circuits invented in 1872 by William Robinson are the most widely used equipment for train navigation systems. They are used for detection of train's occupancy on railway tracks, however, they provide low navigational accuracy. Similarly, tachometers are widely used for many train navigation systems, however, the cumulative tachometer error becomes significant as time passes and as wheel slip and slide occurs in practice [3].

Nowadays higher accuracy in the train navigation systems is the key enabler of the operational safety and efficiency, new services for customers, and low maintenance cost [4]. The above two navigation sensor systems can not meet the needs of high accuracy for the advanced train navigation systems. To achieve the higher accuracy and stability of the train navigation system, there has been a number of studies, among which satellite-based navigation systems have received a great attention; GPS-based train navigation systems have been realized in various forms [5-10]. However, GPS signals may become easily unavailable in tunnels and urban canyons, which can degrade the performance of the GPS-based train navigation system dramatically [11,12]. To cope with the GPS outage, train navigation systems are often equipped with inertial navigation system (INS) [4,5]. However, a commercial-grade INS suffers from cumulative position error when it is used alone for a long time without GPS corrections, so that the combination of GPS and INS does not guarantee high accuracy and stability in a long time GPS outage. Therefore, a highly accurate and stable train navigation system should rely on various sensors to increase the diversity of positioning techniques, and techniques for multisensor data fusion have been investigated in a number of studies [6-10]. For example, some studies proposed train navigation systems based on the centralized Kalman filter using multiple sensor measurements for the RUNE project in 2003 [7], however, the theoretical analysis was not very sufficient.

Recently, a high-speed train with the maximum speed of 430km/h, HEMU-430X, has been developed by the Korean Railroad Research Institute and Hyundai Rotem Inc. In this paper, we propose a high accuracy navigation system for high-speed trains (HANST) such as HEMU-430X based on multisensor data fusion algorithm with non-holonomic constraints and an orthogonal projection map matching algorithm. The federated Kalman filter technique is adopted for the sensor fusion with non-

Manuscript received June 23, 2014; revised October 28, 2014; accepted December 15, 2014. Recommended by Associate Editor Hongbo Li under the direction of Editor Fuchun Sun.

This research was supported by a grant from Railroad Technology Research Program (Technology development on the positioning detection of railroad with high precision) funded by Ministry of Land, Infrastructure and Transport.

Kwanghoon Kim is with LIG Nex1. Inc., Seongnam, Korea, 463-400 (e-mail: khkim73@kaist.ac.kr).

Sanghwan Seol is with Agency for Defense Development (ADD), Daejeon 305-600, Korea (e-mail: ssh03@add.re.kr).

Seung-Hyun Kong is with the CCS Graduate School for Green Transportation, Korea Advanced Institute of Science and Technology (KAIST), Daejeon 305-701, Korea (e-mail: skong@kaist.ac.kr).

* Corresponding author.

holonomic constraints. Local filters are developed using appropriate error models for the various sensors. Especially, to cope with the performance degradation in the GPS outage, RFID tags are deployed along the railway tracks and a novel local filter for RFID positioning is developed. Also, a novel orthogonal projection map matching algorithm is developed and integrated into the proposed system to further improve the performance. For the performance analysis of the HANST, simulations are carried out for a modeled railway track that has the same geographical characteristics to the real railway tracks for high-speed trains in Korea.

The rest of this paper is organized as follows. In Section 2, train sensor subsystems such as INS, tachometers, Doppler radar, differential GPS (DGPS), and RFID considered to improve the accuracy and stability of the proposed navigation system are briefly introduced. In Section 3, we propose a novel navigation filter with six local filters and a master filter for the HANST. Measurement error models for six local filters are analyzed and derived. A three-step orthogonal projection map matching algorithm is proposed in Section 4 to further improve the performance of the proposed system. Finally, in Section 5, the performance of the HANST using the proposed navigation filter and the map matching algorithm is demonstrated with simulations, and the performance result of the HANST is also analyzed for various environments and system deployment scenarios such as the existence of tunnel, RFID deployment spacing, RFID location uncertainty, and DGPS error. The conclusion of this paper is provided in Section 6.

2. TRAIN SENSOR SUBSYSTEMS

In this section, we introduce sensor subsystems used in the proposed train navigation system.

2.1. Inertial navigation system (INS)

There are two kinds of INS; a gimbaled INS (GINS) and a strap-down INS (SDINS). Both INSs provide the changes of position, velocity, and attitude of a vehicle between consecutive time instants by processing the inertial measurements from accelerometers and gyroscopes [13]. The GINS output is expressed in the navigation frame, so that coordinate transformation matrix is not necessary, and it provides a high accuracy. However, the GINS is expensive, and the required hardware is bulky and heavy. On the other hand, the SDINS output is expressed in the body frame, so that a coordinate transformation matrix is necessary. The hardware of SDINS is small and light, and it is cheaper than the GINS; however, it has lower accuracy than the GINS [13]. Although the GINS shows the better performance, the use of SDINS is steadily increasing due to the much lower cost. Therefore, in this paper, we use the SDINS in the HANST.

2.2. Tachometer

Tachometer is one of the most representative sensors used in a train. It can measure the relative distance and velocity of a train by directly counting the rotations of the wheels, but it suffers from cumulative error like other dead reckoning sensors. Also, wheel slip and slide errors have to be treated appropriately for better performance. In this paper, we use the tachometer as a velocity sensor for a velocity local filter.

2.3. Doppler radar

Doppler radar is a special type of radar that measures Doppler frequency of returning signals and estimates the velocity of a vehicle. The Doppler frequency refers to the difference between the observed frequency and the emitted frequency when the radar is moving. A disadvantage of Doppler radar is that its performance depends on environmental conditions such as weather and the relative motion of ahead objects.

2.4. DGPS (Differential Global Positioning System)

GPS is a satellite navigation system that provides absolute position and time information; if there are four or more visible GPS satellites, user position can be estimated with 5~20m accuracy. The GPS positioning errors are from multiple sources, but some of the errors such as ionospheric and tropospheric delays can be measured at a DGPS reference station and delivered to a user receiver for error correction. Since the HANST needs highly accurate measurements for position and velocity, and the DGPS subsystem can provide position and velocity estimates separately, the proposed system employs two DGPS subsystems which have separate and different local filters.

2.5. RFID (Radio Frequency Identification)

The RFID system consist of tags and a reader. When a tag and the reader is close enough, the tag transmits a signal with its identity as a message and the reader receives the signal and identifies the tag.

In this paper, it is assumed that RFID tags, whose positions are measured and stored in a database in advance, are deployed along railway tracks, and that the RFID reader antenna is installed on the bottom of a train facing the ground. The RFID tags can be considered as a landmark such that the RFID subsystem can be regarded as a position sensor of the HANST, because the reader can find its position from the database instantly when the reader receives a signal from a tag. Depending on the speed of the HANST and the RFID tag spacing, the RFID subsystem receives tag signals at various time intervals, i.e., the RFID update rate is aperiodic. A local filter for the RFID subsystem needs to be able to operate with an aperiodic sensing.

2.6. NHC (Non-Holonomic Constraints)

In addition to the sensor subsystems, we develop algorithmic constraints defined by the dynamics of a train. In train dynamics, a train can not move to the left and right direction in most situations except curved paths. Therefore, it can be assumed that a train has only a velocity in the forward direction and the velocities to

other directions are zero. These constraints can be used as additional velocity measurements for train positioning. In this paper, non-holonomic constraints are used as measurements for one of velocity local filters in the HANST.

3. HIGH ACCURACY NAVIGATION SYSTEM FOR HIGH-SPEED TRAINS (HANST)

In this section, we provide the details of the proposed train navigation filter, and measurement models for the local filters are derived. The proposed navigation filter is based on the federated Kalman filter designed by Carlson, which was proposed to reduce the computational complexity of the centralized Kalman filter and to eliminate the cross correlations among local Kalman filters of the decentralized Kalman filter [14,15].

The proposed navigation filter for the HANST consists of six local filters and a master filter as shown in Fig. 1. Each local filter utilizes a different measurement model related to each sensor, and the master filter combines the estimates from the local filters. The federated Kalman filter has several operational modes depending on the presence of a feedback. In this paper, the no-reset mode, which does not produce a feedback, is considered.

3.1. Navigation algorithm for HANST

The schematic diagram of the proposed navigation filter for the HANST is shown in Fig. 1, where INS is used as a reference sensor; therefore, the system equation of local filters can be expressed with INS. There are two kinds of local filters depending on the information from the measurement; velocity local filters and position local filters. The measurements from tachometers, Doppler radar, NHC, and DGPS (velocity) are used for the velocity local filters, and the measurements from DGPS (position) and RFID are for the position local filters. Each local filter has a unique measurement model for each sensor. However, the state variables of the local filters are the same. The estimates from the local filters are combined in the master filter based on the federated Kalman filtering. The details of the navigation filter are derived in this section.

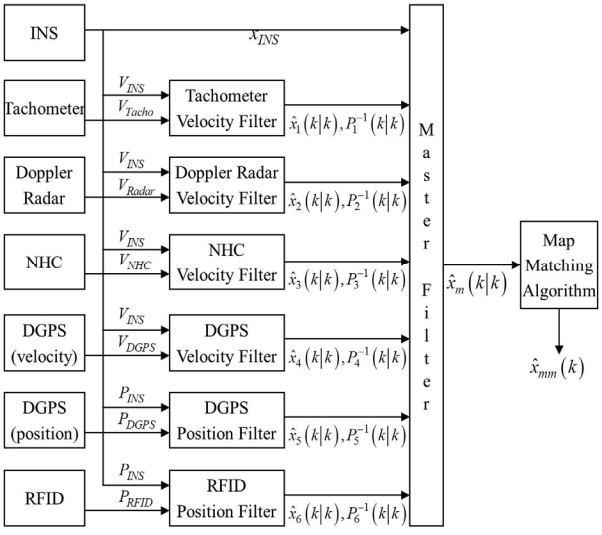

Fig. 1. The navigation filter structure of HANST.

3.2. Local filter design for HANST

3.2.1 System equation for INS

The INS error model can be derived from INS pure navigation equations using the perturbation method [13] and used to derive the system equation of the INS subsystem. The system equation is expressed as

$$\delta\dot{x}(t) = F_{INS}(t)\delta x(t) + G(t)w(t), \tag{1}$$

where F_{INS} is the system matrix, $w(t)$ is a white Gaussian noise with zero mean and covariance $Q(t)$, and $\delta x(t)$ represents the error state of the system. The error state is defined as

$$\delta x(t) = \left[\, \delta P \mid \delta V^n \mid \delta Q_b^n \mid \nabla \mid \eta \,\right]^T, \tag{2}$$

$$w(t) = \left[\, w_a \mid w_g \,\right]^T, \tag{3}$$

where $\delta P = [\delta L\ \delta l\ \delta h]$ are position errors in the ECEF geodetic frame (latitude, longitude, and height), $\delta V^n = [\delta V_N\ \delta V_E\ \delta V_D]$ are velocity errors defined in the navigation frame, $\delta Q_b^n = [\delta q_0\ \delta q_1\ \delta q_2\ \delta q_3]$ is a quaternion error vector, $\nabla = [\nabla_X\ \nabla_Y\ \nabla_Z]$ are accelerometer bias errors in the body frame, and $\eta = [\eta_X\ \eta_Y\ \eta_Z]$ are gyroscope bias errors in the body frame. Accelerometer errors consist of white Gaussian noise $w_a = [w_{aX}\ w_{aY}\ w_{aZ}]$ and bias errors ∇, which are random but assumed constant during the system operation. Similarly, gyroscope errors consist of white Gaussian noise $w_g = [w_{gX}\ w_{gY}\ w_{gZ}]$ and bias errors η, which are random but assumed constant during the system operation.

The system model F_{INS} and $G(t)$ are available from [13] as below.

$$F_{INS} = \left[\begin{array}{c|c|c|c|c} F_{11} & F_{12} & O_{3\times3} & O_{3\times3} & O_{3\times3} \\ \hline F_{21} & F_{22} & F_{23} & F_{24} & O_{3\times3} \\ \hline F_{31} & F_{32} & F_{33} & O_{3\times3} & F_{35} \\ \hline O_{3\times3} & O_{3\times3} & O_{3\times3} & O_{3\times3} & O_{3\times3} \\ \hline O_{3\times3} & O_{3\times3} & O_{3\times3} & O_{3\times3} & O_{3\times3} \end{array}\right], \tag{4}$$

$$G(t) = \begin{bmatrix} O_{3\times3} & O_{3\times3} \\ C_b^n & O_{3\times3} \\ O_{3\times3} & -C_b^n \\ O_{3\times3} & O_{3\times3} \\ O_{3\times3} & O_{3\times3} \end{bmatrix}, \tag{5}$$

where $O_{m\times n}$ is a $m\times n$ zero matrix and C_b^n is a coordinate transformation matrix that represents the rotational transformation from the body frame to the navigation frame.

3.2.2 Measurement equation for tachometers

The measurement for a tachometer velocity filter is the velocity of a train observed in the body frame. A

coordinate transformation matrix is needed because the reference velocity information of INS is obtained in the navigation frame. Therefore, the measurement equation for velocity sensors can be expressed as

$$\begin{aligned} z_{sensor}(t) &= C_n^b\left[V_{INS}^n\right]-\left[V_{Sensor}^b\right] \\ &= H_{sensor}\delta x(t)+v_{sensor}(t), \end{aligned} \tag{6}$$

where $v_{sensor} \sim N(0, R_{sensor})$ denotes that v_{sensor} is a white Gaussian noise with zero mean and covariance $R_{sensor}(t)$. Note that $z_{sensor}(t)$ in (6) is expressed in the body frame where V_{Sensor}^b denotes the velocity of a sensor in the body frame. The velocities in the body frame and the navigation frame are related as

$$V^b = C_n^b V^n, \tag{7}$$

where the transformation matrix C_n^b is defined as

$$C_n^b = \begin{bmatrix} C_{11} & C_{12} & C_{13} \\ C_{21} & C_{22} & C_{23} \\ C_{31} & C_{32} & C_{33} \end{bmatrix}. \tag{8}$$

When the perturbation method [13] is used for (7), the perturbed velocity in the body frame is expressed as

$$\begin{aligned} \hat{V}^b &= V^b + \delta V^b \\ &= \hat{C}_n^b \hat{V}^n \\ &= C_n^b (I+E^n)(V^n+\delta V^n) \\ &= C_n^b V^n + C_n^b E^n V^n + C_n^b \delta V^n + C_n^b E^n \delta V^n, \end{aligned} \tag{9}$$

where

$$\hat{C}_n^b = C_n^b\left(I+E^n\right) \text{ and } E^n = \begin{bmatrix} 0 & -\varepsilon_D & \varepsilon_E \\ \varepsilon_D & 0 & -\varepsilon_N \\ -\varepsilon_E & \varepsilon_N & 0 \end{bmatrix};$$

the elements, ε_N and ε_E, correspond to the attitude errors with respect to the vertical, the level, or tilt errors, while ε_D represents the error about vertical, the heading or azimuth error [13].

When it is assumed that $C_n^b E^n \delta V^n = 0$, the equation in (9) becomes

$$\delta V^b = C_n^b \delta V^n + C_n^b E^n V^n. \tag{10}$$

Also the tilt angle ε^n can be expressed using the quaternion error as [16]

$$\varepsilon^n = [\varepsilon_N \quad \varepsilon_E \quad \varepsilon_D]^T = -2Y^T(Q_b^n)\delta Q_b^n, \tag{11}$$

where

$$Y\left(Q_b^n\right) = \begin{bmatrix} -q_1 & -q_2 & -q_3 \\ q_o & q_3 & -q_2 \\ -q_3 & q_o & q_1 \\ q_2 & -q_1 & q_o \end{bmatrix}. \tag{12}$$

From (10) and (11), we obtain

$$\begin{aligned} C_n^b E^n V^n &= \begin{bmatrix} C_{11} & C_{12} & C_{13} \\ C_{21} & C_{22} & C_{23} \\ C_{31} & C_{32} & C_{33} \end{bmatrix}\begin{bmatrix} 0 & -\varepsilon_D & \varepsilon_E \\ \varepsilon_D & 0 & -\varepsilon_N \\ -\varepsilon_E & \varepsilon_N & 0 \end{bmatrix}\begin{bmatrix} V_N \\ V_E \\ V_D \end{bmatrix} \\ &= -2\begin{bmatrix} C_{13}V_E - C_{12}V_D & C_{11}V_D - C_{13}V_N & C_{12}V_N - C_{11}V_E \\ C_{23}V_E - C_{22}V_D & C_{21}V_D - C_{23}V_N & C_{22}V_N - C_{21}V_E \\ C_{33}V_E - C_{32}V_D & C_{31}V_D - C_{33}V_N & C_{32}V_N - C_{31}V_E \end{bmatrix} \\ &\quad \begin{bmatrix} -q_1 & q_0 & -q_3 & q_2 \\ -q_2 & q_3 & q_0 & q_1 \\ -q_3 & -q_2 & q_1 & q_0 \end{bmatrix}\delta Q_b^n. \end{aligned} \tag{13}$$

From (6), (10), and (13), H_{sensor} can be derived as

$$H_{sensor} = \begin{bmatrix} O_{3\times 3} & C_n^b & H_s & O_{3\times 6} \end{bmatrix}, \tag{14}$$

where

$$\begin{aligned} H_s = & \\ -2&\begin{bmatrix} C_{13}V_E - C_{12}V_D & C_{11}V_D - C_{13}V_N & C_{12}V_N - C_{11}V_E \\ C_{23}V_E - C_{22}V_D & C_{21}V_D - C_{23}V_N & C_{22}V_N - C_{21}V_E \\ C_{33}V_E - C_{32}V_D & C_{31}V_D - C_{33}V_N & C_{32}V_N - C_{31}V_E \end{bmatrix} \\ &\begin{bmatrix} -q_1 & q_0 & -q_3 & q_2 \\ -q_2 & q_3 & q_0 & q_1 \\ -q_3 & -q_2 & q_1 & q_0 \end{bmatrix}. \end{aligned} \tag{15}$$

Since tachometers can measure the velocity in the forward direction of a train (i.e., x-axis), the tachometer measurement equation can be found as

$$\begin{aligned} z_{Tacho}(t) &= C_n^b\left[V_{INS,X}^n\right]-\left[V_{Tacho,X}^b\right] \\ &= H_{Tacho}\delta x(t)+v_{Tacho}(t), \end{aligned} \tag{16}$$

where $v_{Tacho} \sim N(0, R_{Tacho})$ and

$$H_{Tacho} = \left[O_{1\times 3} \mid C_n^b(1,:) \mid H_s(1,:) \mid O_{1\times 6}\right].$$

3.2.3 Measurement equation for Doppler radar

Similarly to the tachometer subsystem, the Doppler radar subsystem also measures the velocity in the x-axis. Therefore, the measurement equation can be found as

$$\begin{aligned} z_{Radar}(t) &= C_n^b\left[V_{INS,X}^n\right]-\left[V_{Radar,X}^b\right] \\ &= H_{Radar}\delta x(t)+v_{Radar}(t), \end{aligned} \tag{17}$$

where $v_{Radar} \sim N(0, R_{Radar})$ and

$$H_{Radar} = \left[O_{1\times 3} \mid C_n^b(1,:) \mid H_s(1,:) \mid O_{1\times 6}\right].$$

3.2.4 Measurement equation for NHC

NHC is not based on sensor measurements but provides physical constraints based on the train dynamics. The velocities of the train in the body frame is nearly zero except the velocity along the x-axis such that

$$V_Y^b = V_{NHC,Y}^b \approx 0, \quad V_Z^b = V_{NHC,Z}^b \approx 0. \tag{18}$$

The constraints (18) can be used as a measurement equation for a NHC velocity filter. Since the constraints are defined in the body frame, the measurement equation for NHC is similar to that for tachometers. The measurement exists only in the y-axis and the z-axis as described in (18). Therefore, the second and third rows of H_{sensor} in (14) are used for H_{NHC} as

$$\begin{aligned} z_{NHC}(t) &= C_n^b \begin{bmatrix} V_{INS,Y}^n \\ V_{INS,Z}^n \end{bmatrix} - \begin{bmatrix} V_{NHC,Y}^b \\ V_{NHC,Z}^b \end{bmatrix} \\ &= H_{NHC}\delta x_{INS}(t) + v_{NHC}(t), \end{aligned} \tag{19}$$

where $v_{NHC} \sim N(0, R_{NHC})$ and

$$H_{NHC} = \left[O_{2\times 3} \mid C_n^b(2:3,:) \mid H_s(2:3,:) \mid O_{2\times 6} \right].$$

3.2.5 Measurement equation for DGPS position

While the state variable δP represents a position error, DGPS provides a position estimate P defined in the ECEF geodetic frame. In order to build a measurement equation in the same format to INS, the position difference between INS and DGPS is used as a measurement. Therefore, the measurement equation for the DGPS position filter is defined as

$$\begin{aligned} z_{DGPS\_P}(t) &= [P_{INS}] - [P_{DGPS}] \\ &= H_{DGPS\_P}\delta x(t) + v_{DGPS\_P}(t), \end{aligned} \tag{20}$$

where $v_{DGPS\_P} \sim N(0, R_{DGPS\_P})$ and

$$H_{DGPS\_P} = \begin{bmatrix} 1 & 0 & 0 & O_{1\times 13} \\ 0 & 1 & 0 & O_{1\times 13} \\ 0 & 0 & 1 & O_{1\times 13} \end{bmatrix}.$$

3.2.6 Measurement equation for DGPS velocity

The idea to derive the measurement equation of the DGPS velocity filter is similar to that of the DGPS position filter. Since the measured information is the velocity of a train in the navigation frame, the measurement equation can be built as

$$\begin{aligned} z_{DGPS\_V}(t) &= [V_{INS}] - [V_{DGPS}] \\ &= H_{DGPS\_V}\delta x(t) + v_{DGPS\_V}(t), \end{aligned} \tag{21}$$

where $v_{DGPS\_V} \sim N(0, R_{DGPS\_V})$ and

$$H_{DGPS\_V} = \begin{bmatrix} O_{1\times 3} & 1 & 0 & 0 & O_{1\times 10} \\ O_{1\times 3} & 0 & 1 & 0 & O_{1\times 10} \\ O_{1\times 3} & 0 & 0 & 1 & O_{1\times 10} \end{bmatrix}.$$

3.2.7 Measurement equation for RFID

In general, Kalman filter is updated periodically. However, the RFID position filter of the proposed system is updated irregularly in time when the train speed is varying over time and the RFID tags are located with irregular or regular spacing, which complicates the RFID local filter. To resolve such a problem, the proposed system compensates the RFID position information received from RFID tags as follows

$$P_{RFID} = P_{RFID,tag} + C_n^{llh} V_{INS}^n \Delta T, \tag{22}$$

where P_{RFID} denotes a compensated RFID position defined in the ECEF geodetic frame, $R_{RFID,tag}$ denotes position information transmitted by an RFID tag and is defined in the ECEF geodetic frame, C_n^{llh} denotes a transformation matrix from the navigation frame to the ECEF geodetic frame, and ΔT is the time difference between the signal transmission at the RFID tag and the next update of the RFID local filter right after the signal transmission. Note that the second term in (22) introduces an unknown position error. To compensate the position error during ΔT, an additional position, calculated using the velocity of INS and ΔT, is added to $R_{RFID,tag}$ in order to obtain P_{RFID} as (22).

In practice, it is possible to design the RFID position filter with periodic update time using (22). If the RFID update rate is very slow and there is no input when the RFID position filter is updated, then the time propagation procedure is performed without a measurement update. The measurement equation of the RFID position filter can have a similar format to the DGPS position filter as follows:

$$\begin{aligned} z_{RFID}(t) &= [P_{INS}] - [P_{RFID}] \\ &= H_{RFID}\delta x(t) + v_{RFID}(t), \end{aligned} \tag{23}$$

where $v_{RFID} \sim N(0, R_{RFID})$ and

$$H_{RFID} = \begin{bmatrix} 1 & 0 & 0 & O_{1\times 13} \\ 0 & 1 & 0 & O_{1\times 13} \\ 0 & 0 & 1 & O_{1\times 13} \end{bmatrix}.$$

3.3. Master filter for HANST

In the master filter [14], the expressions for the time propagation update are

$$\hat{x}_m(k+1|k) = f\left(\hat{x}_m(k|k)\right), \tag{24}$$

$$\begin{aligned} P_m(k+1|k) &= \Phi(k+1,k) P_m(k|k) \Phi^T(k+1,k) \\ &\quad + G(k) Q(k) G^T(k). \end{aligned} \tag{25}$$

and the expressions for the measurement update are as follows:

$$P_m^{-1}(k|k) = \sum_{i=1}^{M} P_i^{-1}(k|k), \tag{26}$$

$$\hat{x}_m(k|k) = P_m(k|k)\left[\sum_{i=1}^{M} P_i^{-1}(k|k)\hat{x}_i(k|k)\right]. \tag{27}$$

where $f(\cdot)$ is the nonlinear navigation system function, $\Phi(k+1,k) = \exp[F_{INS}(t_{k+1} - t_k)]$, and M, i and m denote the total number of local filters, the index of the i th local filter, and the master filter, respectively.

4. MAP MATCHING ALGORITHM

The purpose of a map matching algorithm is to achieve a higher accuracy and stable performance by restricting the possible position of a vehicle to the points within a small map segment. For an example, in the car navigation systems, map matching algorithms perform a point-to-point matching between the estimated position and the geometrically possible nearest point on a map [17]. An extension of the point-to-point map matching is the point-to-curve map matching to find the nearest curve on the map that fits with the estimated positions [18]. An extension of the point-to-curve map matching is the curve-to-curve map matching, where the algorithm finds the nearest curve on the map that fits with the estimated positional curve observed from the history of estimated positions [19].

In the literature, various advanced map matching algorithms using Kalman filters or fuzzy theory have been proposed. However, the basic principle of advanced map matching algorithms is similar to that of the curve-to-curve map matching algorithm. To exploit this principle in the train navigation systems, Saab proposed a map matching algorithm that calculates the changing rate of railroad curvature and correlates the angular rate extracted from map database with measurements from gyroscopes and tachometers in the vehicle [1-2]. However, this technique is not suitable for a high-speed train because most high-speed train tracks are straight and have fluent curves. Therefore, we propose a novel orthogonal projection map matching (OPMM) algorithm for high-speed trains in this section. The OPMM algorithm uses map points on a railway map where map points are spaced one meter (1m) apart along railway tracks and have position information defined in the ECEF geodetic frame. The following variables are defined for the proposed OPMM algorithm.

- j : Index of map point $(j = 1, 2, \cdots N)$
- k : Sampling time index of the MF
- Δt : Update time of the MF
- $mp(j)$: The j th map point on railway tracks
- $\hat{x}_{k,p}^{+}$: *A posteriori* position estimate of the MF
- $\hat{x}_{k,v}^{+}$: *A posteriori* velocity estimate of the MF
- $\sigma_{k,v}^{+}$: Standard deviation of $\hat{x}_{k,v}^{+}$
- $\hat{x}_{k,p}^{mm}$: Position estimate calculated by the OPMM
- α_k, β_k : The two closest map points to $\hat{x}_{k,p}^{+}$
- c_k : Central map point of the search area at k
- δ : Design factor to decide the size of the search area
- ceil(x) : Function to round the elements of x to the nearest integers towards infinity
- $\overrightarrow{ab}$: A Euclidean vector which has an initial point a and a terminal point b
- $proj(\overrightarrow{ab}, \overrightarrow{ac})$: The projection of $\overrightarrow{ab}$ onto $\overrightarrow{ac}$
- $\|x\|$: Two norm of x

The OPMM algorithm based on three steps are developed to obtain more accurate position estimate in high-speed trains. In the first step, the search area for the map matching is selected using *a posteriori* velocity estimate of the master filter (MF) and its standard deviation. In the second step, the two closest map points, that are 1m apart, to the *a posteriori* position estimate of the MF are chosen within the search area. Finally, the position of a train on a railway track is calculated by the OPMM algorithm.

4.1. Selecting the search area (Step 1)

The MF of the HANST provides *a posteriori* position estimate. In general, however, *a posteriori* position estimate may not be located at a railway track due to the estimation errors. To obtain more accurate position estimate, we project *a posteriori* position estimate onto the railway track on which the train is running. To find a unit vector on the railway track for projection, first of all, we need to define the search area of map points.

First, the central map point c_k needs to be determined. When $\| \hat{x}_{k,v}^{+} + \sigma_{k,v}^{+} \| \cdot \Delta t$ is assumed to be the maximum distance that the train moves within Δt seconds, c_k can be calculated from $\hat{x}_{k,v}^{+}$ and $\sigma_{k,v}^{+}$ as shown in (28), (29), and (30), where α_{k-1} and β_{k-1} are the two closest map points at $k-1$ and the unit vector $\overrightarrow{\alpha_{k-1}\beta_{k-1}}$ between two map points is used for vector projection at $k-1$. Notice that we may use $2\sigma_{k,v}^{+}$ or $3\sigma_{k,v}^{+}$ instead of $\sigma_{k,v}^{+}$ in (29). However, the performance are very similar and using $\sigma_{k,v}^{+}$ requires least search effort.

Next, the search area centering around c_k is defined in between $mp(l+q-\delta_k)$ and $mp(l+q+\delta_k)$ as shown in (31) where the size of the search area depends on the design factor δ_k, which is chosen by user. Note that the total number of map points in the search area is equal to $2\delta_k + 1$.

- Find the central map point γ_k:
  At $k-1$,

$$\alpha_{k-1} = mp(l), \quad \beta_{k-1} = mp(l+1). \tag{28}$$

  At k,

$$q = \text{ceil}\left(\left\| \hat{x}_{k,v}^{+} + \sigma_{k,v}^{+} \right\| \cdot \Delta t \right), \tag{29}$$

$$c_k = mp(l+q). \tag{30}$$

- Search area:

$$[mp(l+q-\delta_k) \sim mp(l+q+\delta_k)]. \tag{31}$$

4.2. Finding the two closest map points (Step 2)

In this step, we describe an idea to find the two closest map points α_k and β_k to *a posteriori* position estimate at k. To find α_k and β_k, we calculate the distance between *a posteriori* position estimate and map points within the search area (31) and find the map point $mp(m)$ that has the minimum distance as shown in (33). Next, we again calculate the distances for two map points beside $mp(m)$ and find the map point $mp(n)$ with the minimum distance as shown in (34). Finally, we obtain the two closest map points α_k and β_k to *a posteriori* position estimate $\hat{x}_{k,p}^{+}$

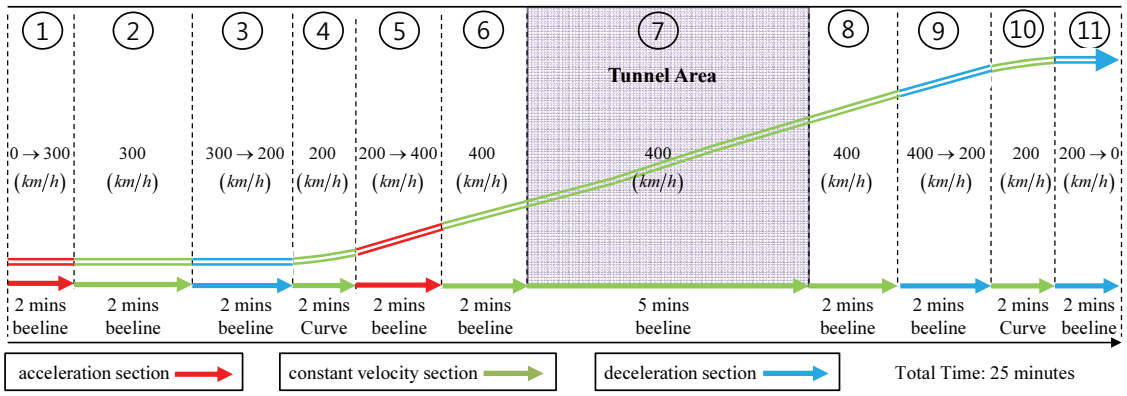

Fig. 2. Train trajectory.

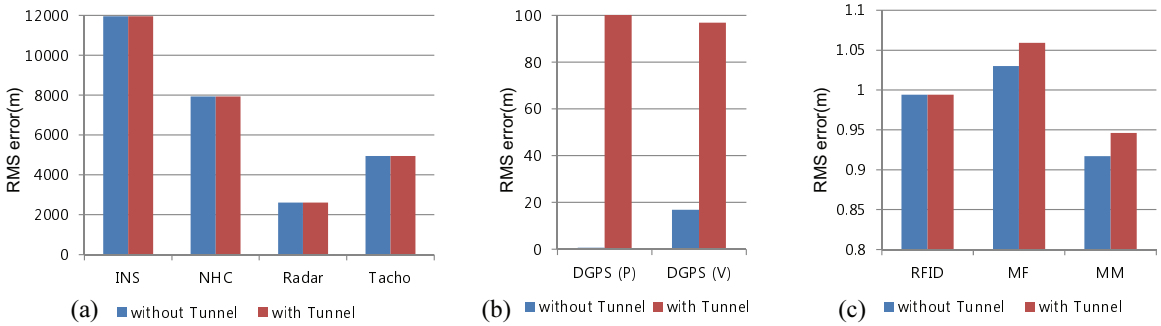

Fig. 3. Performance analysis with respect to existence of tunnel: RMS error (m).

from the selected two map points $mp(m)$ and $mp(n)$. They are defined in (36) and used to make the unit vector for projection in the next step.

- Calculate the distance between $\hat{x}_{k,p}^{+}$ and map points within the search area as follows:

for $i = 1 : 2\delta_k + 1$

$$\text{dist}(i) = \left\| \hat{x}_{k,p}^{+} - mp\left(l + q - \delta_k + i - 1\right) \right\| \tag{32}$$

end

- Find the map point that has the minimum distance:

$$m = \arg\min_{i}[\text{dist}(i)] + l + q - \delta_k - 1, \tag{33}$$

$$n = \arg\min_{p}[\text{dist}(p)] \text{ where } p = m \pm 1, \tag{34}$$

$$l = \min[m, n]. \tag{35}$$

- Find the two closest map points to $\hat{x}_{k,p}^{+}$:

$$\alpha_k = mp(l), \quad \beta_k = mp(l+1). \tag{36}$$

4.3. Projection (Step 3)

We obtain the projected position estimate $\hat{x}_{k,p}^{mm}$. First, we make the unit vector $\overrightarrow{\alpha_k \beta_k}$ from two map points α_k and β_k obtained in (36). Equation (37) shows the projection of *a posteriori* position estimate $\hat{x}_{k,p}^{+}$ onto $\overrightarrow{\alpha_k \beta_k}$. Finally, the position estimate $\hat{x}_{k,p}^{mm}$ calculated by the projection is obtained using (38).

- Project $\hat{x}_{k,p}^{+}$ onto $\overrightarrow{\alpha_k \beta_k}$:

$$proj\left(\overrightarrow{\alpha_k \hat{x}_{k,p}^{+}}, \overrightarrow{\alpha_k \beta_k}\right) = \left(\frac{\overrightarrow{\alpha_k \hat{x}_{k,p}^{+}} \cdot \overrightarrow{\alpha_k \beta_k}}{\left| \overrightarrow{\alpha_k \beta_k} \right|^2} \right) \overrightarrow{\alpha_k \beta_k} \tag{37}$$

- Find $\hat{x}_{k,p}^{mm}$:

$$\hat{x}_{k,p}^{mm} = proj\left(\overrightarrow{\alpha_k \hat{x}_{k,p}^{+}}, \overrightarrow{\alpha_k \beta_k}\right) + \alpha_k. \tag{38}$$

5. PERFORMANCE ANALYSIS

5.1. Simulation conditions

In this section, the performance of the HANST is evaluated with MATLAB simulations. To evaluate the performance for realistic environments, modeling the real high-speed railways is necessary. A pre-survey is carried out to characterize the Korea Train eXpress (KTX) railways, where KTX runs at around 400km/h. As summarized in Table 1, 77.8% of the Seoul-Daejeon KTX railway tracks are straight paths, and the radius of curvature is found to be larger than 7000m. Using Table

Table 1. Seoul-Daejeon KTX railway characteristic.

Radius of curvature (m)	Distance (m)	Percentage of section (%)	Change rate of curvature at 200km/hr (deg/s)
Straight	111221	77.8	
7000	13284	9.3	0.4547
8000	14505	10.1	0.3979
10000	1709	1.2	0.3183
11000	721	0.5	0.2894
15000	1569	1.1	0.2122

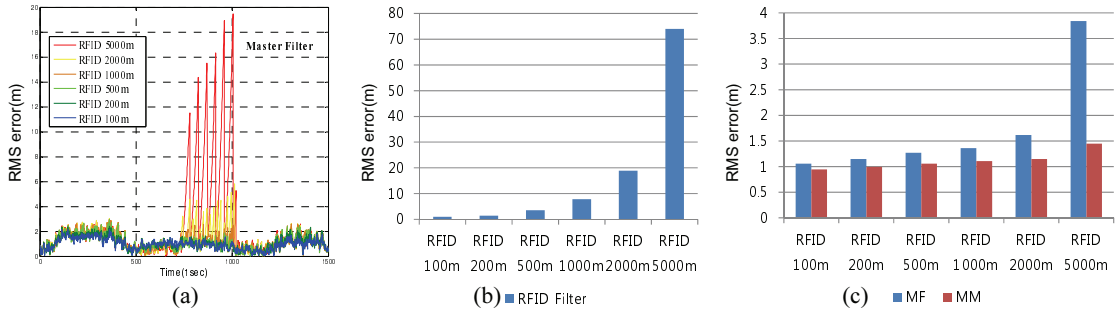

Fig. 4. Performance analysis with respect to RFID deployment spacing: RMS error (m).

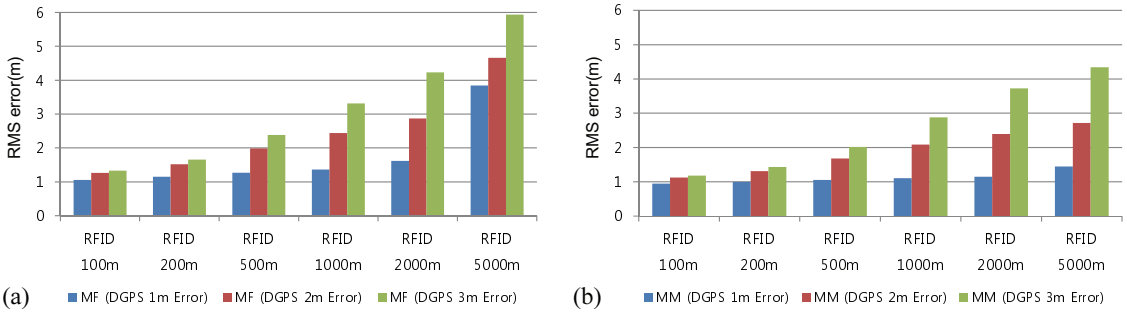

Fig. 5. Performance analysis with respect to DGPS error: RMS error (m).

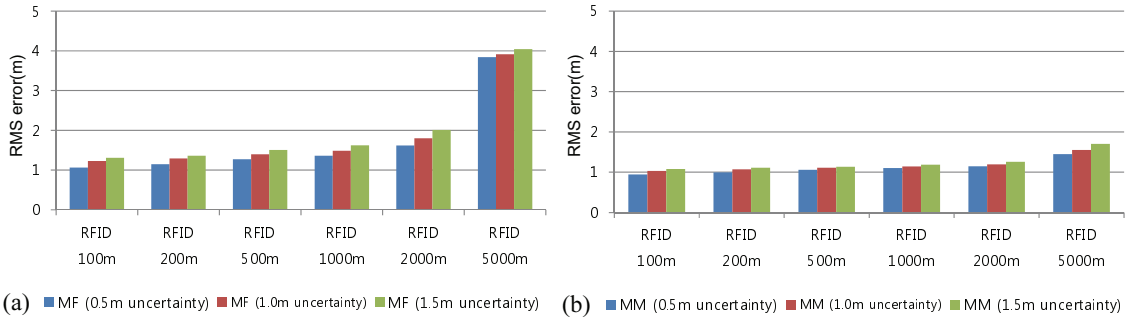

Fig. 6. Performance analysis with respect to RFID location uncertainty: RMS error (m).

1, a railway trajectory for the simulations is designed as illustrated in Fig. 2. The railway trajectory for simulation consists of sections of acceleration, constant velocity, and deceleration. Most of the 11 sections have straight paths, while only two sections (i.e., the fourth and tenth sections) have curved paths, where the train speed is 200km/hr. In the first and fifth sections, the train has accelerations, whereas, in the third, ninth, and eleventh sections, the train has decelerations. In other sections the train has a constant speed. Especially, the train speed is 400 km/h from the sixth to the eighth section. In addition, there is a tunnel of 33,333m long in the seventh section. The overall travel time and distance are 25 minutes and 120km, respectively. The sensor specifications are shown in Table 2. The sensor update rates are different, and the MF has a constant 1Hz update rate that is the common multiple of all sensor update rates. Therefore, when the DGPS with higher update rate is used (e.g., 5Hz or 10Hz), the update rate of the MF should be increased accordingly. And it should be noted that the higher update rate of the MF increases the computational cost of the system almost linearly.

Table 2. Sensor specification.

	Update rate	White Noise (σ)	Random Bias
Accelerometer	100 Hz	50 μg	1000 μg
Gyroscope	100 Hz	0.1 deg/h	1 deg/h
DGPS(position)	1 Hz	1, 2, 3 m	·
DGPS(velocity)	1 Hz	0.5, 1, 1.5 m/s	·
NHC	20 Hz	·	·
Doppler Radar	20 Hz	0.2 m/s	·
Tachometer	20 Hz	0.1 m/s	·
RFID	random	0.5, 1, 1.5 m	·

5.2. Performance analysis

In this section, the performance of the proposed system is analyzed with a number of simulation results. Especially, four simulation scenarios are considered to test the effect of the existence of tunnel, RFID deployment spacing, RFID location uncertainty, and DGPS error on the system performance.

5.2.1 Performance analysis in the tunnel

In general, DGPS can provide accurate position and velocity measurements compared to other sensors, so

that it is an important sensor to maintain small navigation errors. However, it may be unavailable and unreliable in some areas, such as tunnel and urban areas.

In train navigation systems, particularly, signal blockage of DGPS occurs inside tunnels. Fig. 3 shows the effect of the tunnel on the performance of the proposed system with 1m DGPS position error and 0.5m/s DGPS velocity error in open sky environments, 100m RFID deployment spacing, and 0.5m RFID position error. All sensors except the DGPS remain unaffected by the existence of the tunnel as shown in Fig. 3(a). However, two local filters in the DGPS subsystems are degraded dramatically as shown in Fig. 3(b).

For a train navigation system without an RFID subsystem, the performance of the MF is degraded due to the GPS outage, however, when RFID information is available inside the tunnel, it is possible to prevent the monotonous performance degradation although the performance depends on the RFID tag spacing along railway tracks. In case that RFID tags are deployed at every 100m along a railway track, the RFID position filter shows under 1m root mean square (RMS) position error as shown in Fig. 3(c), and the performance of the MF is degraded only slightly. As a result, the RFID subsystem can replace the DGPS subsystem inside tunnels. In addition, Fig. 3(c) shows the result when the proposed OPMM algorithm is applied to the HANST. The HANST with the OPMM algorithm achieves the smaller RMS error compared to the HANST without the OPMM algorithm.

5.2.2 Performance analysis with respect to RFID deployment spacing

As discussed in subsection 5.2.1, the spacing between deployed RFID tags is an important factor to the accuracy and stability of the proposed system. Fig. 4 shows the effect of RFID deployment spacing on the overall performance of the system. Different deployment spacing, such as 100m, 200m, 500m, 1000m, 2000m, and 5000m, are considered for a comparison. Fig. 4 shows that the RMS errors of the RFID position filter and the MF increase with respect to the increase of RFID deployment spacing. However, in case of the OPMM algorithm, it shows only a little difference in accuracy (under 1.5m RMS error) regardless of RFID deployment spacing although it is affected slightly by its spacing, which is because of the RFID location uncertainty that can be caused by RFID location measurement errors propagated into the database and measurement errors occurred in the RFID signal detection.

5.2.3 Performance analysis with respect to DGPS error

DGPS error is also an important factor to the accuracy of the proposed system. In the simulations, it is tested for scenarios that DGPS has 1m, 2m, and 3m position errors and 0.5m/s, 1m/s, and 1.5m/s velocity errors as summarized in Table 2. Fig. 5 shows that the RMS error of the MF with or without the OPMM algorithm increases with respect to the increase of the DGPS error. As shown in Fig. 5(a) and Fig. 5(b), the MF with the OPMM algorithm shows the better performance for all cases than the MF without the OPMM algorithm.

5.2.4 Performance analysis with respect to RFID location uncertainty

RFID location uncertainty is another cause of performance degradation similar to the DGPS error. In the simulations, it is tested that RFID has 0.5m, 1m, and 1.5m position errors as summarized in Table 2. Fig. 6 shows the similar results to the performance results in the subsection 5.2.3. As the RFID location uncertainty increases, the performance of the MF without the OPMM algorithm is degraded as shown in Fig. 6(a). Also the position RMS error of the MF with the OPMM algorithm, as shown in Fig. 6(b), is smaller than the MF without the OPMM algorithm for all cases.

6. CONCLUSION

In this paper, the train navigation system based on a novel navigation filter for sensor fusion and a novel map matching algorithm is proposed. The characteristics of each sensor is investigated to derive the equations of six local filters in navigation filter, and the estimates of the local filters are combined in the master filter. Especially, a novel RFID local filter is developed for irregular RFID measurement updates. Also, a novel three-stage map matching algorithm based on an orthogonal projection is proposed for the proposed system, HANST. The search area of the map matching algorithm is decided using the velocity information from the master filter and a navigation solution at the previous time instance. The map matching algorithm consists of simple three steps, so that this algorithm has a low computational complexity and is suitable for high-speed trains.

In addition, it is considered to use a modeled railway track that has the same geographical characteristics of the railway tracks for high-speed trains in Korea. The performance of the HANST based on a modeled railway track is analyzed by MATLAB simulations. From the simulations, the effects of the existence of tunnel, RFID deployment spacing, RFID location uncertainty, and DGPS error are analyzed for various conditions. Also the simulation results show that the RFID local filter can replace the DGPS filters during the DGPS outage.

It should be noted that the train navigation system based on multiple sensors is vulnerable to sensor faults, for example, slip and slide errors of tachometer which frequently occur during the train's acceleration, deceleration, and moving along a curved railway. Therefore, as a future work, the fault-tolerant train navigation system with a fault-detection scheme should be studied to achieve more reliable and accurate positioning performance.

REFERENCES

[1] S. S. Saab, "A map matching approach for train positioning. part I: development and analysis," *IEEE Trans. on Vehicular Technology*, vol. 49, no. 2, pp. 467-475, March 2000.

[2] S. S. Saab, "A map matching approach for train positioning. part II: application and experimentation," *IEEE Trans. on Vehicular Technology*, vol. 49, no. 2, pp. 476-484, March 2000.
[3] B. Cai, J. Wang, Y. Qin, and J. Liu, "A GNSS based slide and slip detection method for train positioning," *Proc. of Asia-Pacific Conf. Information Processing*, pp. 450-453, 2009.
[4] R. Mázl and L. Přeučil, "Sensor data fusion for inertial navigation of trains in GPS-dark areas," *Proc. of the IEEE Intelligent Vehicles Symposium*, pp. 345-350, 2003.
[5] A. Mirabadi and N. Mort, "Design of fault tolerant train navigation systems," *Proc. of the American Control Conf.*, pp. 104-108, 1999.
[6] A. Mirabadi, F. Schmid, and N. Mort, "Multisensor integration methods in the development of a fault-tolerant train navigation system," *The Journal of Navigation*, vol. 56, pp. 385-398, 2003.
[7] A. Genghi, L. Marradi, L. Martinelli, L. Campa, G. Labbiento, J. Cianci, G. Venturi, G. Gennaro, and M. Tossaint, "The RUNE project: design and demonstration of a GPS/EGNOS-based railway user navigation equipment," *Proc. of ION GPS/ GNSS 2003*, pp. 225-237, September 2003.
[8] H. Zhang, J. Rong, and X. Zhong, "Research of the INS/GPS integrated navigation system for high speed trains," *Proc. of the 9th International Conf. Young Computer Scientists*, pp. 1659-1663, 2008.
[9] J. Liu, B. Cai, T. Tang, and J. Wang, "A CKF based GNSS/INS train integrated positioning method," *Proc. of the IEEE Conf. Mechatronics and Automation*, pp. 1686-1689, 2010.
[10] J. Liu, B. Cai, Y. Wang, J. Wang, and W. Shangguan, "A GPS/compass based train integrated positioning method for high-speed railways," *Proc. of the IEEE-APS Topical Conf. APWC*, pp. 1201-1204, 2012.
[11] S.-H. Kong and W. Nam, "A-GNSS sensitivity for parallel acquisition in asynchronous cellular networks," *IEEE Trans. on Wireless Communications*, vol. 9, no. 12, pp. 3770-3778, December 2010.
[12] S.-H. Kong, "Fast multi-satellite ML acquisition for A-GPS," *IEEE Trans. on Wireless Communications*, vol. 13, no. 9, pp. 4935-4946, September 2014.
[13] D. H. Titterton and J. L. Weston, *Strapdown Inertial Navigation Technology*, Second edition, Institution of Engineering and Technology, 2004.
[14] N. A. Carlson, "Federated square root filter for decentralized parallel processes," *IEEE Trans. on Aerospace and Electronic Systems*, vol. 26, no. 3, pp. 517-524, May 1990.
[15] N. A. Carlson and M. P. Berarducci, "Federated Kalman filter simulation results," *NAVIGATION*, vol. 41, no. 43, pp. 297-321, 1994.
[16] D. Chung, J. G. Lee, C. G. Park, and H. W. Park, "Strapdown INS error model for multiposition alignment," *IEEE Trans. on Aerospace and Electronic Systems*, vol. 32, no. 4, pp. 1362-1366, October 1996.
[17] J. S. Greenfield, "Matching GPS observations to location on a digital map," *Proc. of the 81st Annual Meeting of the Transportation Research Board*, 2002.
[18] C. E. White, D. Bernstein, and A. L. Kornhauser, "Some map matching algorithms for personal navigation assistants," *Transportation Research Part C*, vol. 8, no. 1, pp. 91-108, 2000.
[19] B. P. Phuyal, "Method and use of aggregated dead reckoning sensor and GPS data for map matching," *Proc. of the 15th ITM of Satellite Division of the ION GPS 2002*, pp. 430-437, September 2002.

Kwanghoon Kim received his Ph.D. degree in Electrical Engineering and Computer Science from the Seoul National University in 2006. He is currently working as a research professor at the CCS Graduate School for Green Transportation, Korea Advanced Institute of Science and Technology (KAIST), Daejeon, Korea. His research interests include Fault Detection, Kalman Filtering, GNSS/INS integration system, and GNSS signal processing algorithms.

Sanghwan Seol received his B.S. degree in Mechanical Engineering in 2012 and his M.S. degree from the CCS Graduate School for Green Transportation in 2014, both in the Korea Advanced Institute of Science and Technology (KAIST). He is currently a research engineer at the Raybolt System PMO, Agency for Defense Development (ADD). His research interests include optimal control, detection and estimation for navigation systems.

Seung-Hyun Kong received his B.S. degree in Electronics Engineering from the Sogang University, Korea, in 1992, an M.S. degree in Electrical Engineering from the Polytechnique University, New York, in 1994, and a Ph.D. degree in Aeronautics and Astronautics from the Stanford University, CA, in Jan., 2006. From 1997 to 2004, he was with Samsung Electronics Inc., and Nexpilot Inc., both in Korea, where his research focus was on 2G CDMA and 3G UMTS PHY and mobile positioning technologies. In 2006, he was involved with hybrid positioning technology development using wireless location signature and Assisted GNSS at Polaris Wireless Inc., CA., and from 1997 to 2009, he was a research staff at the corp. R&D, Qualcomm Inc., CA, where his R&D focus was on the indoor location technologies and advanced GNSS technologies. He joined Korea Advanced Institute of Science and Technology (KAIST) in 2010, and he is an associate professor at the CCS Graduate School for Green Transportation at the same institution. His research interests include super-resolution signal processing, detection and estimation for navigation systems, and assisted GNSS in wireless communication systems.